ADVANCED MATERIALS
www.advmat.de

Supramolecular Interface Engineering via Interdiffusion for Reusable and Dismantlable Polymer Adhesion

Kenji Yamaoka, Takuma Wada, Iori Ogasa, Takeru Komyo, Chao Luo, Ryohei Ikura, Masahiro Hino, Masako Yamada, Hideki Seto, Yoshihisa Fujii,* Yasutomo Uetsuji,* and Yoshinori Takashima**

Controllable adhesion that enables both reuse and dismantling is a key requirement for sustainable materials and device integration. Here,a polymeric adhesion system is demonstrated based on reversible interactions at the interface, in which the association and dissociation of supramolecular complexes are externally regulated by thermal and chemical stimuli. By tuning the glass transition temperature (T_g) of the polymers, chain mobility and complex reformation are simultaneously optimized, leading to enhanced interdiffusion and bond recombination at the adhesion interface. Neutron reflectivity (NR) measurements with deuterium labeling revealed that the interfacial width increased with annealing temperature, reaching up to 24.4 nm at 200 °C after 24 hours. The presence of reversible bonds suppressed polymer interdiffusion despite promoting adhesion strength. The resulting materials exhibit excellent reusability and dismantlability under mild stimuli, with strong potential for applications in recyclable electronics, automotive manufacturing, and temporary assembly technologies.

1. Introduction

Reversible and on-demand adhesion is a critical challenge in the development of next-generation materials for sustainable manufacturing, repairable electronics, and modular device integration. Conventional adhesives, once cured, form permanent bonds that impede disassembly, recycling, and material reuse. Thus, designing adhesion systems that combine strong bonding with reversibility under controlled stimuli remains a key goal in materials science. Reusable and dismantlable adhesives have been in high demand to enable controllable adhesion for sustainable material applications.[1–4] Considerable research efforts have been devoted to developing dismantlable adhesion by several researchers. Thermal expanders incorporated into adhesives enable disassembly by inducing rupture of the adhesive layer upon heating.[5–7] The incorporation of easily cleavable covalent bonds into adhesives enables for on-demand debonding via bond scission triggered by thermal, photo, and chemical stimuli.[8–11] A particularly promising strategy for achieving both reusable and dismantlable adhesion involves introducing reversible bonds, such as dynamic covalent bonds and non-covalent interactions, within the adhesion layer or at the

K. Yamaoka, T. Wada, I. Ogasa, R. Ikura, Y. Takashima
Department of Macromolecular Science
Graduate School of Science
The University of Osaka
Toyonaka, Osaka 560-0043, Japan
E-mail: yamaokak23@chem.sci.osaka-u.ac.jp; takasima@chem.sci.osaka-u.ac.jp
K. Yamaoka, R. Ikura, Y. Takashima
Forefront Research Center (FRC)
The University of Osaka
Toyonaka, Osaka 560-0043, Japan

T. Komyo, C. Luo, Y. Uetsuji
Department of Mechanical Engineering
Osaka Institute of Technology
Asahi-ku, Osaka 535–8585, Japan
E-mail: yasutomo.uetsuji@oit.ac.jp
M. Hino
Institute for Integrated Radiation and Nuclear Science
Kyoto University
Kumatori, Osaka 590-0494, Japan
M. Yamada, H. Seto
Institute of Materials Structure Science
High Energy Accelerator Research Organization (KEK)
Tsukuba, Ibaraki 305–0801, Japan
Y. Fujii
Department of Applied Chemistry
Graduate School of Engineering
Mie University
Tsu, Mie 514–8507, Japan
E-mail: fujii@chem.mie-u.ac.jp
Y. Takashima
Institute for Open and Transdisciplinary Research Initiatives (OTRI)
The University of Osaka
Suita, Osaka 565–0871, Japan

The ORCID identification number(s) for the author(s) of this article can be found under https://doi.org/10.1002/adma.202507939

DOI: 10.1002/adma.202507939

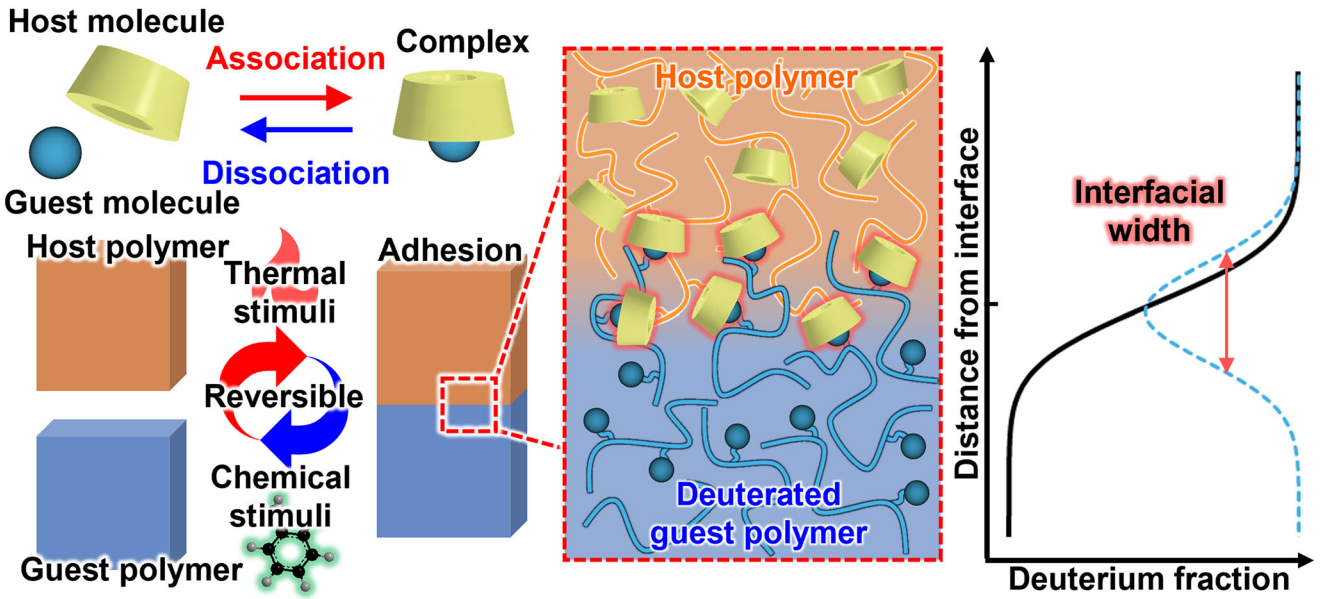

Figure 1. Conceptual image of reusable and dismantlable adhesion through formation of host–guest complexes and interdiffusion at the adhesion interface.

adhesion interface.[12–17] By precisely controlling the association and dissociation of these reversible bonds, reversible adhesion with tunable performance can be realized.

In previous studies, the adhesion between hydrogel/hydrogel and hydrogel/substrate was achieved by host–guest complex formation at the adhesive interface.[18–21] The adhesion via host–guest complexes exhibited reversibility and dismantlability based on molecular recognition of host molecules. However, hydrogels have limited applicability as adhesives due to their poor mechanical strength, and achieving adhesion between solvent-free polymers remains challenging without the use of interfacial solvents.[22] The realization of reversible and dismantlable adhesion via host–guest chemistry remains limited by the efficiency of complex formation at polymer–polymer interfaces. Recent studies have revealed that the recombination of reversible bonds is strongly influenced by the mobility of polymer chains. In particular, tuning the glass transition temperature (T_g) offers a means to control segmental motion, which is essential for efficient bond reformation.[23–25] Considering that adhesion between polymers is achieved by diffusion of chains across the interface,[26–28] we hypothesize that optimization of T_g would simultaneously promote recombination of reversible bonds and enhance interdiffusion at the adhesion interface, thereby enabling the reversible and dismantlable adhesion via host–guest complexes.

The objective of this study is to elucidate how reversible host–guest bonds affect polymer interdiffusion and adhesion performance at chemically identical polymer interfaces, through structural analysis enabled by NR. We prepared host and guest polymers that exhibited adhesion through the host–guest complex formations at the interface, achieved by optimizing the main chain composition to regulate T_g. The adhesion of the polymers was evaluated via tensile testing. NR measurements evaluated the interdiffusion of polymers, employing model systems with well-defined architectures. Although polymer interdiffusion involving reversible bonds has previously been studied using energy-dispersive X-ray spectroscopy (EDX)[29] and atomic force microscopy (AFM),[30] these investigations have primarily focused on interfaces between chemically dissimilar polymers. However, it remains unclear whether reversible bonds promote or hinder chain interdiffusion in chemically identical polymers. We aim to resolve this question through systematic experiments and quantitative interfacial structural analysis using NR. The NR measurements, enabled by deuterium labeling, allow for structural analysis of interfaces between chemically identical polymers. We employed NR to analyze the interfacial structure and investigate the effects of reversible bonds on polymer interdiffusion. The interdiffusion at the adhesion interface was quantitatively analyzed as interfacial width, enabling us to elucidate the impact of reversible bonds on polymer diffusion across the interface. Furthermore, we demonstrated the reusable and dismantlable adhesion by modulating adhesion strength through thermal and chemical stimuli (**Figure 1**).

2. Preparation and Characterization

2.1. Host and Guest Polymers for Adhesion Tests

Host polymers, which copolymerized butyl acrylate (BA), acrylic acid (AA), and Mono-6-*N*-ethyl methacrylamide triacetyl *β*-cyclodextrin (TAc*β*CDMAAm), are denoted as P(BA-AA-*β*CD) (**Figure 2a** and Scheme S1, Supporting Information). The molar ratio of TAc*β*CDMAAm in the host polymer was fixed at 1 mol% in this paper. Guest polymers, which copolymerized with BA, AA, and 1-adamantyl oxy methyl acrylate (Ad), were also prepared by the same methods (Figure 2b and Scheme S2, Supporting Information) using Ad instead of TAc*β*CDMAAm and denoted as P(BA-AA-Ad(x)). x was defined as the mol%

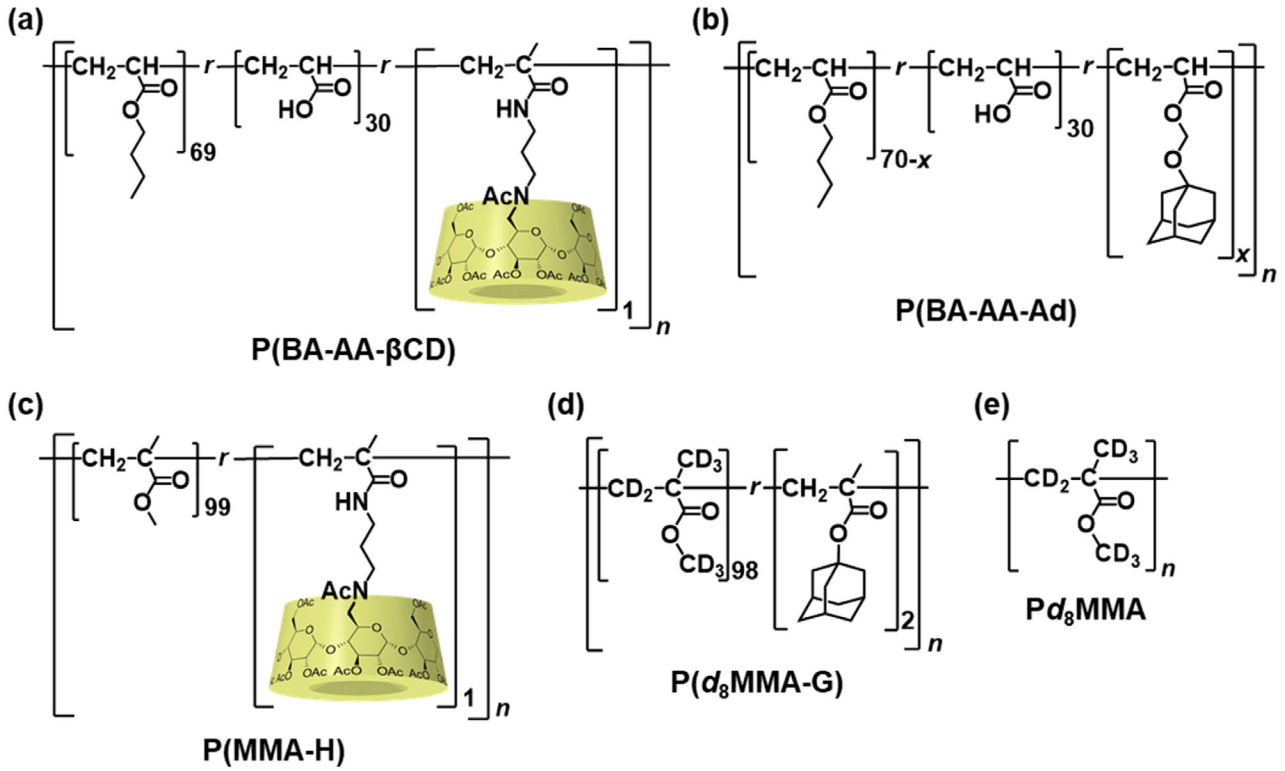

Figure 2. Chemical structures of a) P(BA-AA-βCD), b) P(BA-AA-Ad(x)), c) P(MMA-H), d) P(d_8MMA-G), and e) Pd_8MMA.

of Ad in the guest polymer. The amount of each reagent used in polymerization is summarized in Table S1 (Supporting Information). The mol% of AA in P(BA-AA-βCD) and P(BA-AA-Ad(x)) was fixed at 30 mol% because adjusting a T_g) of the polymers from −10–5 °C (T_g + 30–20 °C ≤ room temperature) allows an adhesion of polymers at room temperature. The chemical structure of host and guest polymers was confirmed by proton nuclear magnetic resonance (^{1}H NMR) spectra in deuterated chloroform ($CDCl_3$) at 30 °C as shown in Figures S1–S5 (Supporting Information). The T_g values were evaluated by differential scanning calorimetry (DSC) (Figure S6, Supporting Information). **Table 1** summarizes T_g of P(BA-AA-βCD) and P(BA-AA-Ad(x)). The numver-average molecular weight (M_n), weight-average molecular weight (M_w), and polydispersity index (M_w/M_n) of P(BA-AA-βCD) and P(BA-AA-Ad(x)) were estimated by comparing them to poly(butyl acrylate) polymerized using the same procedure (Figure S7 and Table S2, Supporting Information).

Table 1. Characteristic properties of P(BA-AA-βCD) and P(BA-AA-Ad(x)).

Polymer	βCD [a] [mol%]	Ad, x [a] [mol%]	T_g [b] [°C]
P(BA-AA-βCD)	1	–	5.2 ± 2.0
P(BA-AA-Ad(0))	–	0	−12.1 ± 1.0
P(BA-AA-Ad(1))	–	1	−6.4 ± 0.6
P(BA-AA-Ad(2))	–	2	−6.7 ± 1.2
P(BA-AA-Ad(3))	–	3	−5.7 ± 0.6

[a] Estimated by ^{1}H NMR in $CDCl_3$ at 30 °C [b] Determined by DSC.

2.2. Host and Guest Polymer for NR Measurements

Acrylate-based polymers with low T_g are not suitable for interfacial structural analysis using NR measurements, as their polymer chains readily diffuse at room temperature and cannot be controlled. Therefore, model polymers with high T_g are required for accurate NR measurements. We selected poly(methyl methacrylate) (PMMA) for the model polymer for the following reasons. i) PMMA has a high T_g. ii) Deuterated MMA is available. iii) PMMA is insoluble in water when making bilayer films by the floating method.

Host polymers were synthesized by copolymerizing methyl methacrylate (MMA) and TAcβCDMAAm, and designated as P(MMA-H) (Figure 2c and Scheme S3, Supporting Information). The mol% of TAcβCDMAAm in the host polymer was fixed at 1 mol%. Deuterated polymers were also prepared by the same method by using deuterated methyl methacrylate (d_8MMA) instead of MMA (Schemes S4,S5, Supporting Information). Guest polymers, which copolymerized with d_8MMA and 1-adamantyl methacrylate (AdMA), and a homopolymer of d_8MMA were denoted as P(d_8MMA-G) and Pd_8MMA, respectively (Figure 2d,e). The mol% of AdMA in the guest polymer was fixed at 2 mol%. The feed composition used for the polymerizations is summarized in Table S3 (Supporting Information). The actual molar ratio of host and guest molecules in the products was characterized by ^{1}H NMR spectra in $CDCl_3$ at 30 °C, as shown in Figures S8–S11 (Supporting Information). M_n, M_w, and M_w/M_n were polystyrene standard values determined by gel permeation chromatography (GPC) in tetrahydrofuran (THF) at 40 °C (Figure S12, Supporting Information). The T_g values were determined

Table 2. Characteristic properties of P(MMA-H), P(d_8MMA-G), and Pd_8MMA.

Polymer	H[a)] [mol%]	G[a)] [mol%]	M_n[b)] [kg/mol]	M_w[b)] [kg/mol]	M_w/M_n[b)]	R_g[c)] [nm]	T_g[d)] [°C]
P(MMA-H)	1	–	20.9	31.4	1.57	4.4	117.0 ± 1.0
P(d_8MMA-G)	–	2	20.0	28.6	1.51	4.2	117.4 ± 0.3
Pd_8MMA	–	–	16.8	24.8	1.48	3.9	113.7 ± 0.4

[a)] Estimated by ^{1}H NMR in $CDCl_3$ at 30 °C; [b)] Determined by GPC(polystyrene standards) in THF at 40 °C; [c)] $R_g = 0.025 \times M_w^{1/2}$[32]; [d)] Determined by DSC.

by DSC (Figure S13, Supporting Information). Those values of P(MMA-H), P(d_8MMA-G), and Pd_8MMA are summarized in **Table 2**. M_n of these polymers were more than twice the entanglement molecular weight of a syndiotactic-rich PMMA (M_e = 9.1 kg mol^{-1}),[31] and these polymers have entanglements. The radius of gyration (R_g) of the polymers were determined from the literature.[32] T_g of Pd_8MMA was 3.7 °C lower than that of P(d_8MMA-G).

3. Results and Discussion

3.1. Effect of Adhesion Time, Temperature, and Guest Molecule Concentration on the Adhesion Strength

A sandwich specimen was prepared as shown in **Figure 3a** to measure the adhesion strength between P(BA-AA-βCD) and P(BA-AA-Ad(x)). Rectangular pieces of P(BA-AA-βCD) and P(BA-AA-Ad(x)) films were freshly cut, and a single P(BA-AA-Ad(x)) piece was placed between two P(BA-AA-βCD) pieces. The adhesive interfaces were welded under various annealing times and temperatures. During tensile testing, the P(BA-AA-Ad(x)) piece predominantly elongated as shown in Figure 3b, due to its lower Young's modulus compared to P(BA-AA-βCD) (Figure S14, Table S4, and Movie S1, Supporting Information). Consequently, the initial length of the P(BA-AA-Ad(x)) piece was defined as L_0, its elongated length as L, allowing the calculation of strain ($\epsilon = (L\text{-}L_0)/L_0$). Stress ($\sigma$) was determined by dividing the applied load (N) by the cross-sectional area (A) of the P(BA-AA-Ad(x) piece ($\sigma = N/A$). All stress-strain (S-S) curves used to evaluate adhesion strength and toughness are provided in Figures S15-S17 (Supporting Information).

The S-S curves of adhesion test specimens with x = 0 and 2 mol% after annealing at 25 °C or 80 °C for 24 h are shown in Figure 3c. The corresponding adhesion strength and toughness values, derived from these S–S curves, are presented in Figure 3d,e. Even in the absence of complex formation at the adhesion interface (x = 0 mol%), the pieces adhered through the van der Waals force of BA[24,33,34] and hydrogen bonding of AA. The adhesion strength at x = 0 mol% exhibited a slight increase after annealing at 80 °C for 24 h. In contrast, when the complexes were present at the adhesion interface (x = 2 mol%), annealing at 80 °C for 24 h significantly increased stress at the high ϵ, resulting in enhanced adhesion strength and toughness. We conducted molecular dynamics (MD) simulations to demonstrate that host–guest complexed form at the adhesion interface. Two polymer models based on MMA were prepared for comparison: PMMA-H/PMMA-G and PMMA/PMMA. In addition, the ratio of complex formation (c) between host and guest molecules was set to 0% or 100% in the PMMA-H/PMMA-G model to investigate its effect on mechanical properties (Figures S18–S21, Supporting Information). The presence of host–guest complexes as reversible cross-links (c = 100%) resulted in higher stress at larger strain. On the other hand, the PMM-H/PMMA-G with c = 0% and PMMA/PMMA did not show an increase in stress at large strain. These simulation results are consistent with our experimental findings on the adhesion strength of P(BA-AA-Ad(x))/P(BA-AA-βCD) (Figure 3c), where the σ value increased when polymers contained host and guest molecules and were annealed at 80 °C for 24 h. Therefore, the increased stress at high strain suggests complex formation at the adhesion interface.

We examined the effects of annealing time (t), annealing temperature, and guest molecule concentration (x) on adhesion strength. The adhesion strength between P(BA-AA-βCD) and P(BA-AA-Ad(2)) after annealing at 80 °C exhibited a $t^{1/4}$ dependence up to 24 h (Figure 3f), suggesting that polymer self-diffusion across the adhesion interface contributed to the increase in adhesion strength. Previous studies on polymer healing efficiency[29,35–37] have reported a similar $t^{1/4}$ dependence for tensile strength recovery, as both adhesion and healing are governed by polymer self-diffusion across the interface and can be predicted using the reptation model.[38–41] The same dependence of the adhesion strength on the annealing time was observed at the annealing temperature of 120 °C (Figure S22, Supporting Information). Polymer interdiffusion typically follows segmental diffusion with a $t^{1/4}$ dependence for $t < \tau_r$, where τ_r is the time required for a chain to escape from its tube. In contrast, self-diffusion, characterized by conventional Fickian diffusion, follows a $t^{1/2}$ dependence for $t > \tau_r$.[42–44] Notably, adhesion and polymer recovery can be achieved through segmental diffusion within relatively short times ($t < \tau_r$) without requiring Fickian diffusion at longer times ($t > \tau_r$). The observed plateau in adhesion strength at extended annealing times indicates that the interfacial structure reached equilibrium at 80 °C. Increasing the annealing temperature further enhanced adhesion strength (Figure 3g), and the maximum adhesion strength achieved at 120 °C approached the intrinsic tensile strength of P(BA-AA-Ad(2)). Additionally, the adhesion strength reached its peak at x = 2 mol% (Figure 3h), correlating with the tensile strength of P(BA-AA-Ad(x)) (Table S4, Supporting Information).

3.2. Interfacial Structure via NR and Interdiffusion of Polyers with Host–Guest Complexes

NR measurements were conducted for a quantitative analysis of polymer diffusion behavior at the adhesion interface using model polymers optimized for NR analysis. Spin-coated bilayer films on

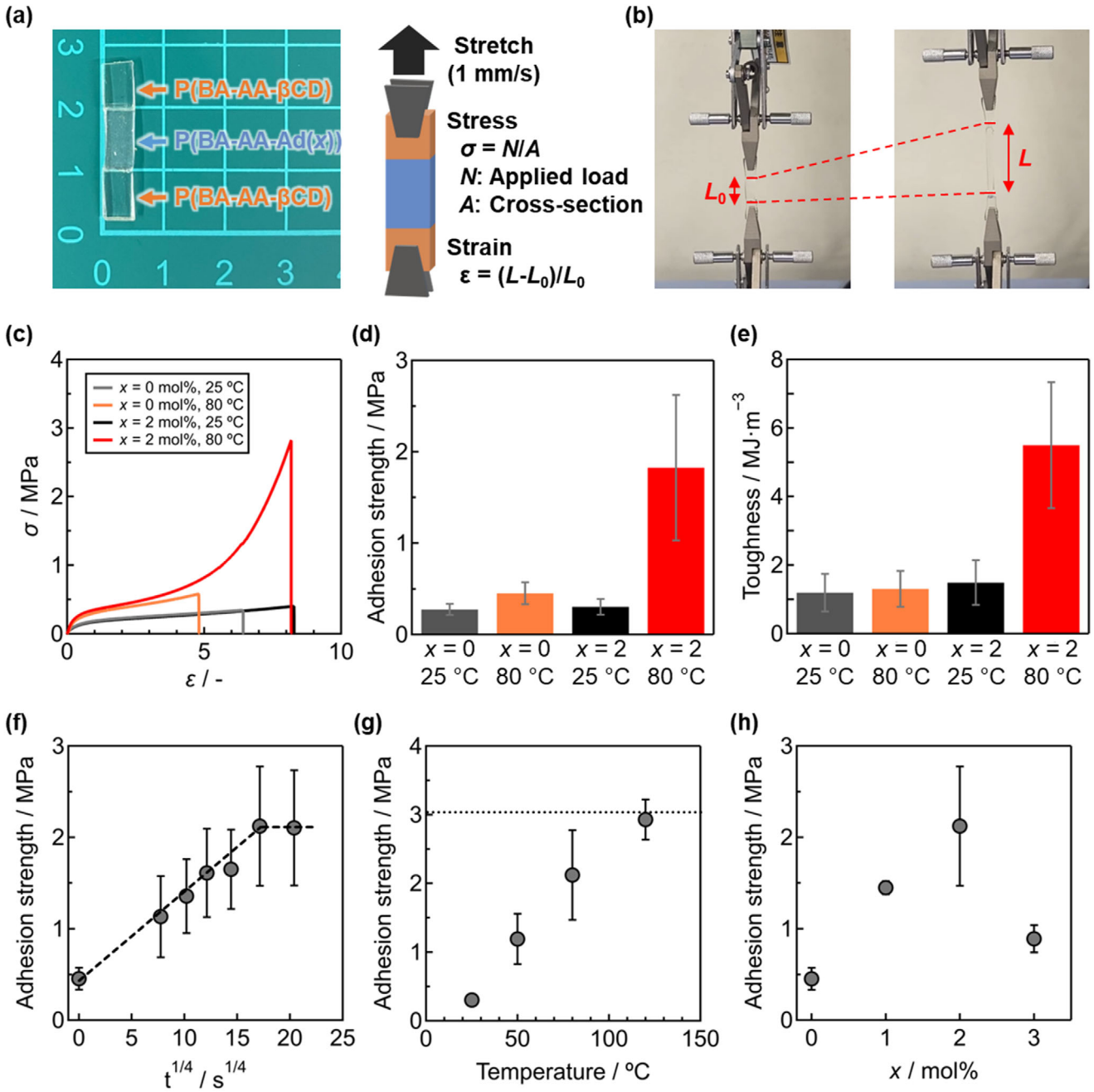

Figure 3. a) Procedure of tensile tests for evaluation of adhesion strength. b) Snapshots of the tensile tests of adhesion specimens. c) Stress–Strain curves, d) adhesion strength, and e) toughness compared with P(BA-AA-Ad(0))/P(BA-AA-βCD) and P(BA-AA-Ad(2))/P(BA-AA-βCD) specimens after annealing at 25 °C and 80 °C. f) Annealing time and g) temperature dependence of adhesion strength of P(BA-AA-Ad(2))/P(BA-AA-βCD). h) The x dependence of adhesion strength. The black dashed line in panel (f) is guided to the eye. The black dotted line in panel g) is the intrinsic tensile strength value of P(BA-AA-Ad(2)).

the Si substrate were prepared to measure the interfacial width between the host and guest polymers (**Figure** 4a). The flotation method was employed to fabricate bilayer films to detect subtle changes in the interfacial width.[45,46] Figure S23 (Supporting Information) shows detailed procedures for preparing the bilayer films. The NR technique allows for the evaluation of interfacial width at the polymer/polymer interface by selectively deuterating one of the polymers.[46–48] Figure 4b presents the schematic of bilayer films, consisting of a 50 nm thick of P(MMA-H) at the bottom layer and a 100 nm thick of P(d_8MMA-G) at the top layer. It is well known that substrate and chain confinement effects significantly influence when the thickness is below $\approx 3R_g$, where R_g denotes the radius of gyration of the polymer chain.[49–54]

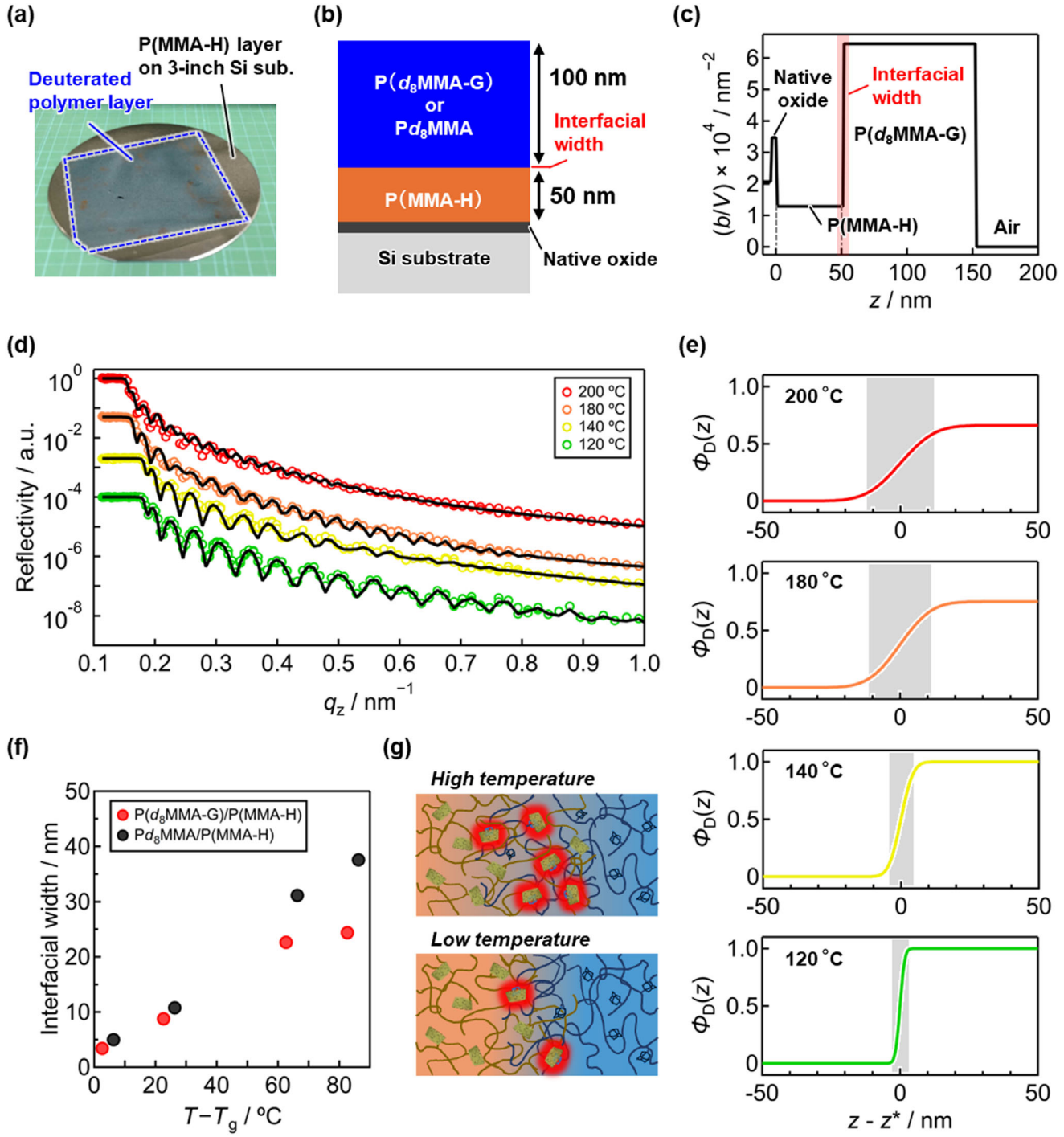

Figure 4. a) Optical image of bilayer films for NR measurements. b) Cross-section and c) model (b/V) profile for the NR analysis. d) NR curves and e) volume fraction distribution of the deuterated polymer ($\Phi_D(z)$) of the P(d_8MMA-G)/P(MMA-H) bilayer films after annealing at various temperatures. The gray highlight represents the interfacial width. f) Annealing temperature dependence of the interfacial width. g) Schematic image of the adhesion interface. The complexes formed at the interface are indicated in red.

In this study, we assumed that these effects would not influence interdiffusion behavior at the selected film thickness. The initial thickness of each layer before annealing was determined via X-ray reflectivity (XR) measurements (**Figure S24**, Supporting Information). The model neutron scattering length density (b/V) profile used for fitting the NR curves is shown in Figure 4c and plotted as a function of the perpendicular distance (z) from the interface between the Si substrate and the native oxide layer. Assuming symmetric polymer interdiffusion, the (b/V) profile at the P(MMA-H)/P(d_8MMA-G) interface was described by an error

function[26,55,56] and the interfacial width value was defined as the standard deviation of the error function.

Simulations of the NR curve based on the model (b/V) profile (Figure 4c) were conducted to predict the impact of increasing the interfacial width on the NR curves (Figure S25, Supporting Information). The amplitude of the Kiessig fringes was anticipated to diminish with increasing interfacial width. The NR curves for the P(d_8MMA-G)/P(MMA-H) bilayer films annealed at temperatures above T_g for 24 h (Figure 4d). Experimental data are depicted as symbols, while solid lines represent the best-fit calculated reflectivity based on the model (b/V) profiles (Figures S26,S27, Supporting Information). The detailed fitting parameters for all samples are summarized in Tables S5–S12 (Supporting Information). The calculated NR curves demonstrated good agreement with the experimental data, suggesting that the model (b/V) profiles accurately reflect the compositional distribution in the film along the axis normal to the interface. As predicted from the simulations, the amplitude of the Kiessig fringes in the experimental data diminished with increasing annealing temperature, indicating an increase in interfacial width. Figure 4e illustrates the volume fraction distribution of the deuterated polymer ($\Phi_D(z)$) at the P(MMA-H)/P(d_8MMA-G) interface, calculated from the model (b/V) profiles at each annealing temperature (Equation S1, Supporting InformationSupporting Information). The horizontal axis represents the distance $z - z^*$, relative to the total thickness of the native oxide and the P(MMA-H) layer, where z^* denotes the position of P(MMA-H)/P(d_8MMA-G) interface. The interface became increasingly diffuse with higher annealing temperature. Figure 4f shows the annealing temperature dependence of interfacial width. The interfacial width of P(d_8MMA-G)/P(MMA-H) bilayer expanded with rising annealing temperature due to enhanced interdiffusion, reaching a value of 24.4 nm at 200 °C. This interfacial width value was comparable to that typically observed in the welding of glassy polymers.[27,28]

Comparing the interfacial width value with and without the guest molecular elucidated the influence of complex formation at the interface on the interdiffusion of polymers (Figure 4f). The horizontal axis shows the annealing temperature (T) relative to the T_g of P(d_8MMA-G) and Pd_8MMA, respectively. In the absence of the guest molecule, no host–guest complexes formed at the interface between P(MMA-H) and Pd_8MMA. Near T_g (120 °C and 140 °C), the interfacial width of Pd_8MMA/P(MMA-H) was slightly larger than that of P(d_8MMA-G)/P(MMA-H) due to the lower T_g of Pd_8MMA (3.7 °C lower) and its higher segmental mobility. At elevated annealing temperatures (180 °C and 200 °C), the interfacial width of P(d_8MMA-G)/P(MMA-H) was significantly smaller than that of Pd_8MMA/P(MMA-H). The reversible bonds present in the side chains delay terminal relaxation beyond the lifetime of the reversible bond while increasing the self-diffusion coefficient (D_s) of the polymer.[57–59] Consequently, the host–guest complex formation at the interface hindered polymer interdiffusion, resulting in a reduced interfacial width for P(d_8MMA-G)/P(MMA-H). The D_s of polymers were estimated from the MD simulation (Figures S28–S32, Supporting Information). Two polymer models based on MMA were prepared for comparison: PMMA-H/PMMA-G and PMMA-H/PMMA. No clear difference of the D_s values of PMMA-H/PMMA-G and PMMA-H/PMMA below or near T_g. In contrast, above T_g, the D_s values of PMMA-H/PMMA-G were significantly lower than those of PMMA-H/PMMA. A lower D_s value corresponds to slower diffusion, resulting in a smaller interfacial width at the same annealing temperature. Thus, the simulation predictions qualitatively agree with the experimental results for the interfacial width (Figure 3f).

This reduced interfacial width aligns with the observation that the enhanced adhesion strength between P(BA-AA-Ad(2))/P(BA-AA-βCD) arises from not only polymer interdiffusion but also from complex formation at the adhesion interface.

Finally, we compared the interfacial width of P(d_8MMA-Ad)/P(MMA-βCD) and the adhesion strength of P(BA-AA-Ad(2))/P(BA-AA-βCD) (Figure 3g) to examine the correlation between interfacial structure and adhesion strength. Both the interfacial width and adhesion strength increased with higher annealing temperatures within the temperature range studied. Elevated annealing temperatures enhanced polymer interdiffusion, broadening the interfacial region where host and guest polymers interpenetrated. This broader interface promoted the formation of host–guest complexes, leading to increased adhesion strength (Figure 4g).

3.3. Reusable and Dismantlable Adhesions

Adhesion techniques that allow repeated sticking and peeling are in high demand for industrial applications. The adhesion of P(BA-AA-βCD) and P(BA-AA-Ad(x)) demonstrated reusability through the reversible formation of host–guest complexes at the adhesion interface. **Figure 5a** shows the experimental procedure to evaluate this repeatability. Initially, the adhesion test specimen underwent a tensile test. When the specimen broke at the adhesion interface, the separated pieces were reattached, and annealed at 80 °C for 24 h, and subjected to a second tensile test. This cycle of re-adhesion and tensile testing was repeated five times. The S-S curves of the P(BA-AA-Ad(2)/P(BA-AA-βCD) for each cycle are displayed in Figure 5b, showing nearly identical shapes across cycles. The adhesion strength and toughness derived from these S-S curves (**Figure S33**, Supporting Information) are presented in Figure 5c,d, respectively. The recovery ratio of adhesion strength remained between 78% and 94%, while that of toughness was between 79% and 87%. These results indicate that the host–guest complex-based adhesion system maintains its adhesive performance over multiple cycles. Modulating the thermal mobility of polymers facilitated the association and dissociation of host–guest complexes at the interface, enabling repeatable adhesion. However, the adhesion strength depends on the T_g of polymers. Altering T_g influences both the complex formation behavior and mechanical properties, emphasizing the need to optimize T_g based on the intended adhesion strength and function. These adhesion materials show potential for use in temporary fixing adhesions during electronic devices manufacturing. Additionally, annealing at higher temperatures can be employed to enhance adhesion strength when a more robust bond is needed.

The adhesion of P(BA-AA-βCD) and P(BA-AA-Ad(x)) can be easily dismantled using a chemical stimulus. Chemical inhibitors were introduced at the adhesion interface to cleave the host–guest complexes (**Figure 6a** left). Water (H_2O), chloroform ($CHCl_3$), and toluene were used as inhibitors. Toluene

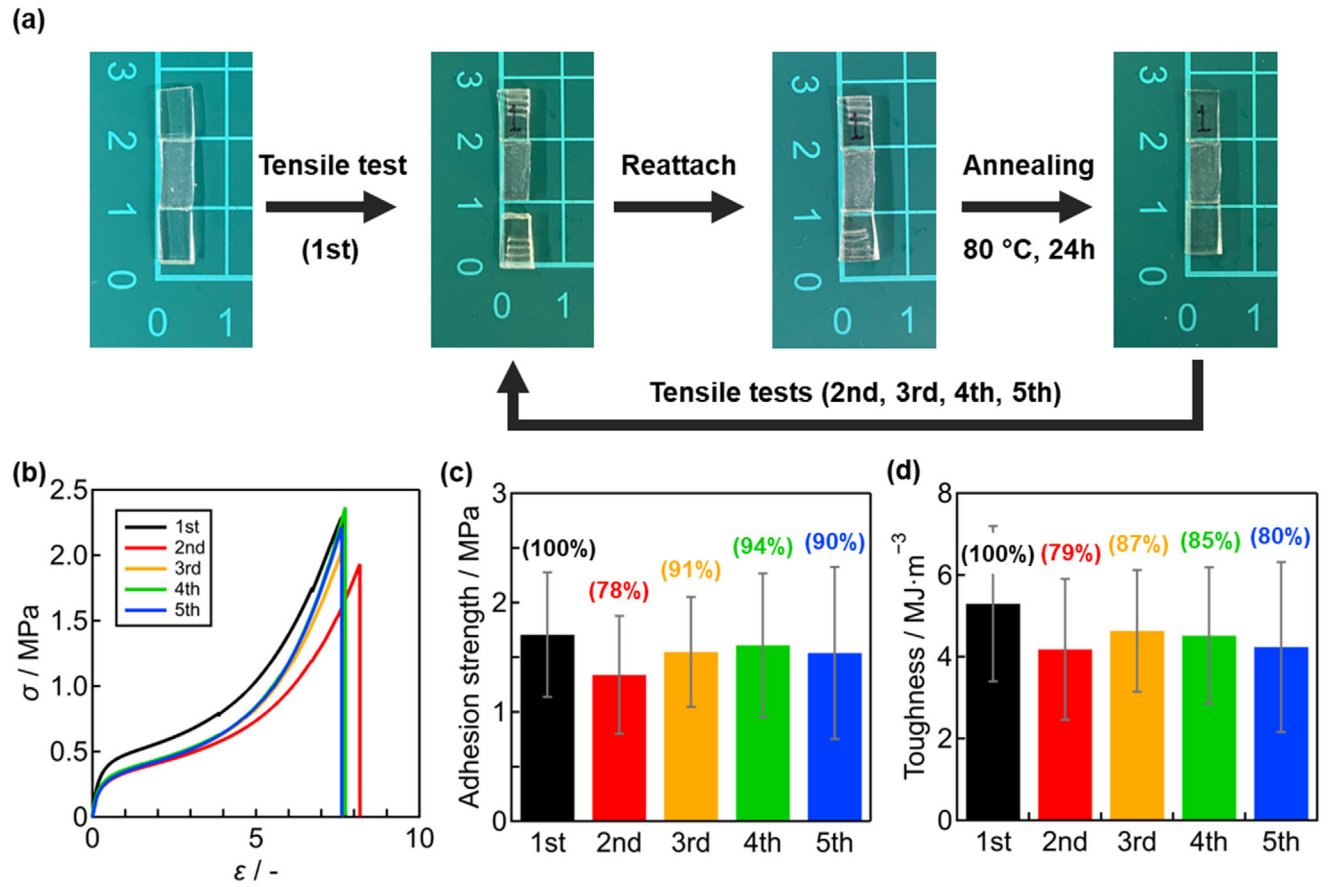

Figure 5. a) Experimental procedure of reusability. b) Stress–Strain curves, c) adhesion strength, and d) toughness of the adhesion specimens with P(BA-AA-βCD) and P(BA-AA-Ad(2)) at each cycle number. The figure in brackets means the recovery ratio based on the pristine value.

and other aromatic molecules can be encapsulated in the βCD cavity. The high molecular mobility of small molecules compared to the Ad molecules anchored to the side chain enables the formation of new complexes between βCD and toluene, which cleaves the reversible bonds between βCD and Ad at the adhesion interface. While H_2O and $CHCl_3$ dissolve the polymers at the adhesion interface, they do not inhibit complex formation. The S-S curves of P(BA-AA-Ad(2))/P(BA-AA-βCD) after applying the inhibitors to the adhesion interface are shown in Figure 6b and Figure S34 (Supporting Information). Dropping H_2O and $CHCl_3$ reduced the adhesiveness of P(BA-AA-Ad(2))/P(BA-AA-βCD). The changes in adhesion strength and toughness after applying the inhibitors are shown in Figure 6c,d. The figures in brackets represent the reduction ratio of adhesion strength and toughness after applying the inhibitors relative to pristine values. With H_2O and $CHCl_3$, the adhesion strength decreased to 41% and 46%, respectively. However, adding toluene resulted in a dramatic reduction of adhesion strength to 15%. A similar trend was observed for toughness when toluene was applied. These results suggest that by adding the appropriate chemical inhibitor, the host–guest complexes at the adhesion interface can be dissociated, enabling easily dismantling of the bond. These findings indicate that adhesion strength and provides a useful method for reversible adhesion in various applications.

Removal of the inhibitor from the adhesion interface enabled the re-adhesion of P(BA-AA-Ad(2))/P(BA-AA-βCD) as shown in Figure 6a, right. The volatile inhibitors, such as toluene, were eliminated by annealing or vacuum drying. The S-S curves for P(BA-AA-Ad(2))/P(BA-AA-βCD) after removing the inhibitors are shown in Figures 6e and S35 (Supporting Information). The elongation of adhesion specimens returned to the pristine level upon removal of the inhibitor, indicating that the adhesion properties were regained. The changes in adhesion strength and toughness after removing the inhibitors are shown in Figure 6f,g. The values in parentheses represent the recovery ratio of adhesion strength and toughness based on pristine values. When applying toluene as an inhibitor, the adhesion strength decreased significantly. However, after removing toluene, the adhesion strength was restored to 63% by annealing and 76% by vacuum drying. A similar trend was observed in the recovery of toughness after removing toluene.

The complex formation at the adhesion interface was successfully modulated by the addition and removal of the inhibitor, enabling easy dismantling via chemical stimuli. The appropriate inhibitor to dissociate the complexes dramatically decreased the adhesion strength, and the adhesion strength was restored by the removal of the inhibitor. These findings demonstrate the potential of this approach for the on-demand disassembly of the adhesion systems and reuse of substrate materials.

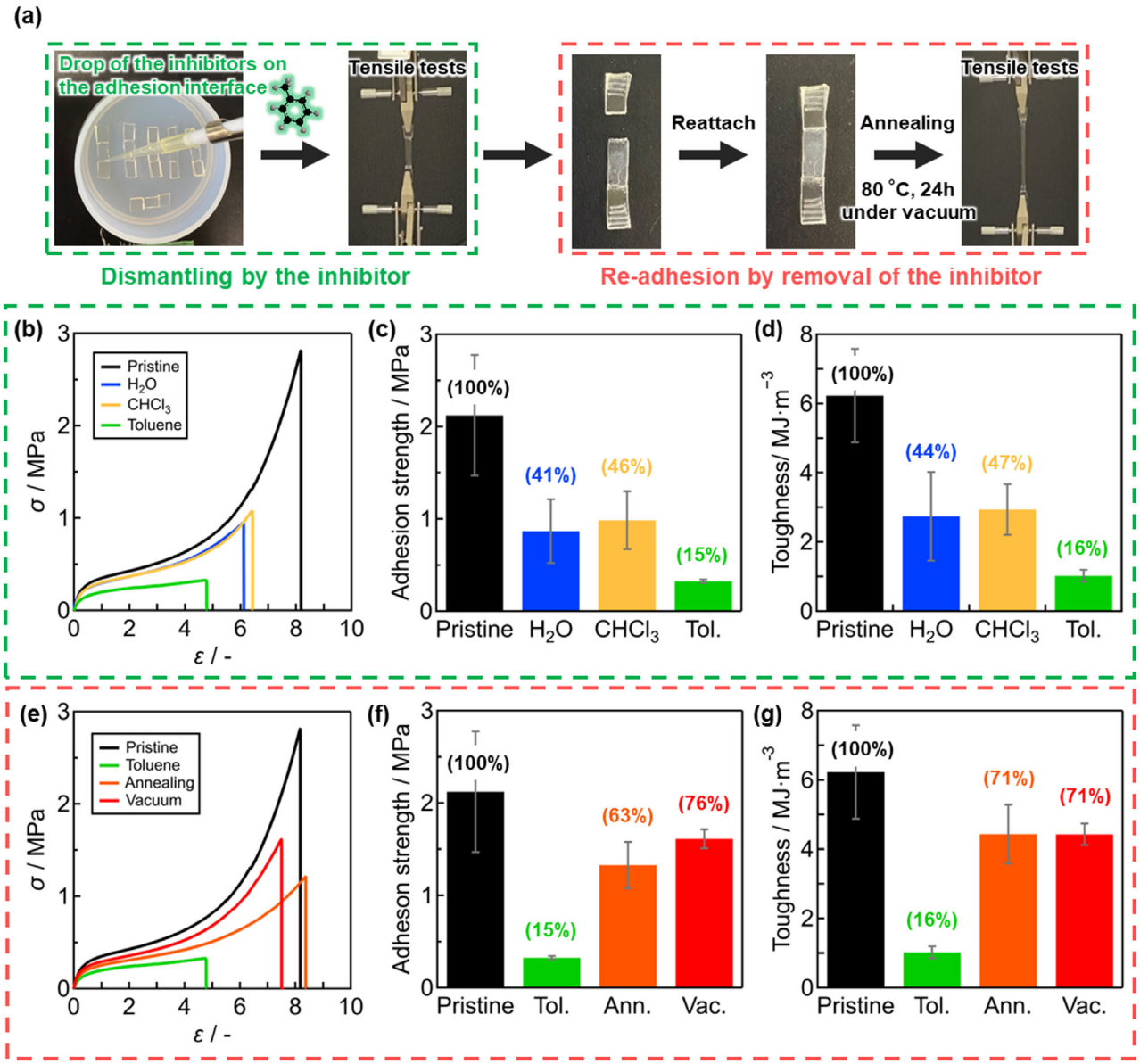

Figure 6. a) Experimental procedure of stimuli responsibility. b) Stress-Strain curves, c) adhesion strength, and d) toughness of the adhesion specimen with P(BA-AA-βCD) and P(BA-AA-Ad(2)) dismantling by the inhibitor. e) Stress–Strain curves, f) adhesion strength, and g) toughness of the adhesion specimen with P(BA-AA-βCD) and P(BA-AA-Ad(2)) in re-adhesion by removal of the inhibitor. The figure in brackets means the reduction and recovery ratio based on the pristine value.

4. Conclusion

In this study, we developed a reusable and dismantlable adhesion system by integrating reversible host–guest interactions and polymer interdiffusion at the adhesion interface. By tuning the T_g of the polymers, we were able to modulate segmental mobility and thereby enhance the recombination of reversible bonds and the diffusion of polymer chains across the interface. The association and dissociation of the host–guest complexes were successfully controlled through thermal and chemical stimuli, enabling both repeatable and on-demand dismantlable adhesion.

NR measurements, combined with deuterium labeling, allowed for quantitative analysis of the interfacial width, which increased with annealing temperature and reached 24.4 nm after 24 h at 200 °C. Notably, although the presence of reversible bonds hindered polymer interdiffusion and resulted in a thinner interface, the overall adhesion strength was enhanced due to the formation of reversible bonds at the interface. Furthermore, the application and subsequent removal of a chemical inhibitor demonstrated that adhesion strength could be reversibly modulated through complex dissociation and reformation.

These findings provide fundamental insights into the interplay between reversible bonding and polymer diffusion in adhesion systems and establish practical design principles for the development of sustainable, reusable, and dismantlable adhesive materials. Such systems are expected to find significant applications

in fields requiring temporary or reconfigurable adhesion, including automotive manufacturing, electronic device fabrication, and circular materials engineering.

5. Experimental Section

Materials: BA, AA, MMA, phenyl bis(2,4,6-trimethyl benzoyl)phosphine oxide (BAPO), 2,2′-Azobis(isobutyronitrile) (AIBN), toluene, THF, and chloroform were purchased from Nacalai Tesque Inc. TAcβCDMAAm was purchased from Kyoeisha Chemical Co., Ltd. Ad and AdMA were purchased from Osaka Organic Chemical Industry Ltd. d_8MMA was purchased from Polymer Source. Inc. $CDCl_3$ stabilized with silver foil with 0.03% tetramethylsilane (TMS) was purchased from Eurisotop. MMA was purified by passing over a short column of activated basic alumina to remove the polymerization inhibitor and dried in a molecular sieve. Other reagents were used as received. De-ionized water was obtained by Milli-Q system, MilliporeSigma.

Methods—1H NMR Spectroscopy: Pro^{1}H NMR spectra were recorded in $CDCl_3$ at 30 °C with a JEOL ECZR ECA500 NMR spectrometer at 500 MHz. Chemical shifts were referenced to an internal standard for TMS ($\delta = 0$ ppm).

Methods—GPC: GPC measurements were performed using HLC-8420GPC EcoSEC (Tosoh Co.) with THF as eluent at 40 °C with two columns (Tosoh TSK gel SuperHZM-N ×2). A refractive index detector was utilized to determine M_n, M_w, and M_w/M_n. The molecular weights were estimated from a calibration curve measured for polystyrene (PS) standards (Tosoh Co.).

Methods—DSC: T_g of polymers was measured by DSC200 and DSC7020 system (Hitachi High-Technologies Co.) with N_2 gas flow (50 mL mi^{-1}n). For P(BA-AA-βCD) and P(BA-AA-Ad(x)) polymers, the temperature increased to 50 °C in the first heating scan at the heating rate of 10 °C/min to remove thermal history in advance, then decreased from 50 °C to −80 °C at the cooling rate of 5 °C/min and increased from −80 °C to 50 °C in the second heating scan at the same heating rate. For P(MMA-H), Pd_8MMA, and P(d_8MMA-G) polymers, the temperature increased from 30 °C to 200 °C in the first heating scan at the heating rate of 10 °C/min to remove thermal history in advance, then decreased from 200 °C to 30 °C at the cooling rate of 5 °C/min and increased from 30 °C to 200 °C in the second heating scan at the same heating rate. The T_g value was determined as the middle point of the onset and offset temperatures of the baseline shift upon glass transition at the second heating scan and was measured three times for each polymer. The average of these measurements was taken as the T_g value, and the standard deviation was used as the uncertainty.

Methods—Tensile Test: Tensile tests of the polymers were performed by using Autograph AG-X plus (Shimadzu Co.). Engineering stress and strain were recorded at a deformation rate of 1 mm s^{-1}. The dimension of the adhesion specimen for the tensile test is shown in Figure S36 (Supporting Information). The adhesion specimen was prepared by sandwiching one guest polymer piece between two host polymer pieces. Adhesion strength was defined as the stress at rupture. Toughness was determined as the area between the S-S curve and the strain axes.

Methods—NR: A neutron reflectometry experiment was conducted using Soft Interface Analyzer (SOFIA) at BL16,[60,61] Materials and Life Science Facility, Japan Proton Accelerator Research Complex (J-PARC), Tokai, Ibaraki, Japan and Multilayer Interferometer and reflectometer for Neutrons (C3-1-2, MINE) at Japan Research Reactor-3 (JRR-3), Tokai, Ibaraki, Japan. Specular reflectivity was measured from the bilayer films on a 3-inch Si substrate, with incident neutron angles (θ) and wavelength (λ) set to $\theta = 0.30°$, 0.70°, and 1.80° with $\lambda = 0.20$–0.88 nm for SOFIA, and $\theta = 0.5°$–5° with $\lambda = 0.88$ nm for MINE. The beam footprint was chosen from the fully covered areas and set to 20 mm in width and 30 mm in length. The neutron momentum transfer perpendicular to the interface (q_z) was defined as $q_z = (4\pi/\lambda)\sin\theta$. Neutron incidence was directed from the free surface. The scattering density (b/V) profile normal to the substrate surface was computed by fitting the reflectivity spectra using the MOTOFIT program.[62] Reflectivity spectra were fitted with a multilayer model comprising silicon, native oxide, P(MMA-H), and the deuterated polymer (P(d_8MMA-G) or Pd_8MMA). The (b/V) values of silicon, native oxide, P(MMA-H), P(d_8MMA-G), and Pd_8MMA were 2.07×10^{-4}, 3.47×10^{-4}, 1.29×10^{-4}, 6.35×10^{-4}, and 6.45×10^{-4} nm^{-2}, respectively. The thickness of each layer was predetermined through X-ray reflectivity measurements. The interfacial width was defined as $\sigma\sqrt{2\pi}$, where σ is a parameter indicating interfacial roughness between host and guest polymers, and obtained by fitting the NR curves with an error function profile implemented in the MOTOFIT program. σ is the standard deviation of the Gaussian function. The detailed fitting parameters for all samples are summarized in Tables S5–12 (Supporting Information).

Methods—XR: XR measurements were performed by Automated Multipurpose X-ray Diffractometer (SmartLab, Rigaku holdings Co.). X-ray was produced by a Cu Kα radiation ($\lambda = 0.154$ nm) at 45 keV and 200 mA. The XR curves were recorded between $2\theta = 0.01°$ and 2°. The thickness of polymer films on the Si substrate were determined by fitting analysis based on the model density (ρ) profile of the samples.

Methods—MD Simulation: All-atom MD simulations were performed to investigate the mechanical properties and D_s of polymers with reversible bonds. All models were created in Materials Studio software (BIOVIA Inc.). All MD simulations were carried out using the Large-scale Atomic/Molecular Massively Parallel Simulator (LAMMPS) software package.[63]

In this study, the Consistent Valence Force Field (CVFF) was employed to describe the interatomic interactions.[64,65] The non-bonded interactions consist of van der Waals forces and electrostatic interactions. The van der Waals interactions were modeled using the Lennard–Jones (LJ) 12–6 potential.[63] Electrostatic interactions were treated using the Particle–Particle Particle-Mesh (PPPM) method to efficiently handle long-range Coulombic forces. All simulations were performed under periodic boundary conditions to ensure the homogeneity and physical validity of the system. Details of the force field used in the MD simulation are described in Supporting Information (Equations S2–S7, Supporting Information).

In uniaxial tensile simulations, two models of PMMA-H/PMMA-G and PMMA/PMMA were prepared to compare mechanical properties. The all-atom model of PMMA-H/PMMA-G consisted of 10 PMMA-H chains (Degree of polymerization (N) = 50, molar ratio of host molecules = 2 mol%) and 10 PMMA-G chains (N = 50, molar ratio of guest molecules = 4 mol%), for a total of 20 linear chains. In addition, the ratio of complex formation of host and guest molecules (c) in the model was set to 0% or 100% to compare the effects of the complex formation on mechanical properties. The all-atom model of PMMA/PMMA consisted of 20 PMMA chains (N = 50). The chemical structure of polymers consisted MMA, TAcβCDMAm as a host molecule, and AdMA as a guest molecule. The uniaxial tension was carried out under the NPT ensemble with a tensile rate of 1×10^{-6} s^{-1} to obtain the stress (σ) – strain (ϵ) curve.

In diffusion simulations, two models of PMMA-H/PMMA-G and PMMA-H/PMMA were prepared to confirm the effects of reversible bonds on D_s. The all-atom model of PMMA-H/PMMA-G consisted of 10 PMMA-H chains (N = 50, molar ratio of host molecules = 2 mol%) and 10 PMMA-G chains (N = 50, molar ratio of guest molecules = 4 mol%), for a total of 20 linear chains with c = 100%. The all-atom model without of PMMA-H/PMMA consisted of 10 PMMA-H chains (N = 50, molar ratio of host molecules = 2 mol%) and 10 PMMA chains (N = 50), for a total of 20 linear chains. The D_s values were calculated as a mean-square displacement (MSD)[66] for all atoms at various temperatures from 300 K to 500 K as follows.

$$\mathrm{MSD}\ (t) = \frac{1}{N}\sum_{i=1}^{N} \left| r_i\ (t) - r_i\ (0) \right|^2 \tag{1}$$

$$D_s = \frac{1}{2} \times \frac{1}{3} \times \frac{\mathrm{dMSD}\ (t)}{dt} \tag{2}$$

here, N, r_i, and t represent a degree of polymerization, an atomic posion, and time, respectively.

Supporting Information

Supporting Information is available from the Wiley Online Library or from the author.

Acknowledgements

This work was supported by the JST Core Research for Evolutional Science and Technology (CREST) program JPMJCR22L4 (Y.T.); JSPS KAKENHI Grant Number JP25K18079; the Suzuki Foundation; and Tokuyama Science Foundation (K.Y.). The NMR and XR measurements were performed at Analytical Instrument Facility, Graduate School of Science, The University of Osaka. The NR experiments at the Materials and Life Science Experimental Facility of the J-PARC were performed under a user program (Proposal No. 2023B0322). This work was carried out by the JRR-3 general user program managed by the Institute for Solid State Physics, the University of Tokyo (Proposal No. 24576).

Conflict of Interest

The authors declare no conflict of interest.

Data Availability Statement

The data that support the findings of this study are available in the supplementary material of this article.

Keywords

dismantlable, interdiffusion, neutron reflectivity, polymer adhesion, reusable, reversible bond

Received: April 26, 2025
Revised: August 16, 2025
Published online:

[1] A. Matsumoto, *Polym. J.* **2024**, *56*, 223.
[2] A. Sierra-Romero, K. Novakovic, M. Geoghegan, *Langmuir* **2022**, *38*, 15476.
[3] Y. Qian, S. Kosaba, R. Ikura, K. Yamaoka, Y. Takashima, *Polym. J.* **2025**, *57*, 491.
[4] K. R. Mulcahy, A. F. R. Kilpatrick, G. D. J. Harper, A. Walton, A. P. Abbott, *Green Chem.* **2022**, *24*, 36.
[5] Y. Nishiyama, N. Uto, C. Sato, H. Sakurai, *Int. J. Adhes. Adhes.* **2003**, *23*, 377.
[6] C.-H. Stamp, J. Stumpp, C. Calvino, *Adv. Mater.* **2025**, *37*, 2414308.
[7] A. Schmid, L. R. Sutton, S. P. Armes, P. S. Bain, G. Manfrè, *Soft Matter* **2009**, *5*, 407.
[8] E. Sato, H. Tamura, A. Matsumoto, *ACS Appl. Mater. Interfaces* **2010**, *2*, 2594.
[9] M. Iseki, Y. Suzuki, H. Tachi, A. Matsumoto, *ACS Omega* **2018**, *3*, 16357.
[10] Y. Matsumura, K. Yamaoka, R. Ikura, Y. Takashima, *ACS Appl. Mater. Interfaces* **2025**, *17*, 20261.
[11] Y. Gao, K. Wu, Z. Suo, *Adv. Mater.* **2019**, *31*, 1806948.
[12] M. Aizawa, H. Akiyama, Y. Matsuzawa, *Adv. Eng. Mater.* **2022**, *24*, 2100823.
[13] M. Kobayashi, M. Terada, A. Takahara, *Soft Matter* **2011**, *7*, 5717.
[14] M. Kobayashi, A. Takahara, *Polym. Chem.* **2013**, *4*, 4987.
[15] T. J. Gately, W. Li, S. H. Mostafavi, C. J. Bardeen, *Macromolecules* **2021**, *54*, 9319.
[16] S. Lamping, L. Stricker, B. J. Ravoo, *Polym. Chem.* **2019**, *10*, 683.
[17] M. Aizawa, H. Akiyama, Y. Matsuzawa, A. Shishido, *Polym. J.* **2024**, *56*, 401.
[18] A. Harada, R. Kobayashi, Y. Takashima, A. Hashidzume, H. Yamaguchi, *Nat. Chem.* **2011**, *3*, 34.
[19] M. Osaki, T. Sekine, H. Yamaguchi, Y. Takashima, A. Harada, *ACS Appl. Polym. Mater* **2021**, *3*, 2189.
[20] Y. Takashima, Y. Shojima, T. Sekine, M. Osaki, Y. Kobayashi, H. Yamaguchi, T. Sekito, K. Hatano, K. Nakajima, A. Harada, *Chem. Lett.* **2018**, *47*, 1255.
[21] Y. Takashima, T. Sahara, T. Sekine, T. Kakuta, M. Nakahata, M. Otsubo, Y. Kobayashi, A. Harada, *Macromol. Rapid Commun.* **2014**, *35*, 1646.
[22] T. Kakuta, Y. Takashima, T. Sano, T. Nakamura, Y. Kobayashi, H. Yamaguchi, A. Harada, *Macromolecules* **2015**, *48*, 732.
[23] Y. Zhou, J. Wen, Y. Nie, *Macromolecules* **2024**.
[24] Y. Zhao, H. Wu, R. Yin, K. Matyjaszewski, M. R. Bockstaller, *ACS Macro Lett.* **2024**, *13*, 1.
[25] J.-M. Park, C. S. Park, S. K. Kwak, J.-Y. Sun, *Sci. Adv.* **2024**, *10*, adp0729.
[26] P. F. Green, E. J. Kramer, *Macromolecules* **1986**, *19*, 1108.
[27] R. Schnell, M. Stamm, C. Creton, *Macromolecules* **1998**, *31*, 2284.
[28] R. Schnell, M. Stamm, C. Creton, *Macromolecules* **1999**, *32*, 3420.
[29] L. N. Neumann, E. Oveisi, A. Petzold, R. W. Style, T. Thurn-Albrecht, C. Weder, S. Schrettl, *Sci. Adv.* **2021**, *7*, abe4154.
[30] C. B. Cooper, S. E. Root, L. Michalek, S. Wu, J.-C. Lai, M. Khatib, S. T. Oyakhire, R. Zhao, J. Qin, Z. Bao, *Science* **2023**, *380*, 935.
[31] S. Wu, R. Beckerbauer, *Polym. J.* **1992**, *24*, 1437.
[32] J. M. O'Reilly, D. M. Teegarden, G. D. Wignall, *Macromolecules* **1985**, *18*, 2747.
[33] M. W. Urban, D. Davydovich, Y. Yang, T. Demir, Y. Zhang, L. Casabianca, *Science* **2018**, *362*, 220.
[34] H. Lai, C. Jin, J. Park, R. Ikura, Y. Takashima, M. Ouchi, *Angew. Chem., Int. Ed.* **2023**, *62*, 202218597.
[35] R. P. Wool, K. M. O'Connor, *J. Appl. Phys.* **1981**, *52*, 5953.
[36] Y. H. Kim, R. P. Wool, *Macromolecules* **1983**, *16*, 1115.
[37] A. M. Grande, S. J. Garcia, S. van der Zwaag, *Polymer* **2015**, *56*, 435.
[38] P. G. de Gennes, *J. Chem. Phys.* **1971**, *55*, 572.
[39] M. Doi, S. F. Edwards, *J. Chem. Soc., Faraday Trans. 2* **1978**, *74*, 1789.
[40] P. G. de Gennes, *Phys. Today* **1983**, *36*, 33.
[41] M. Doi, S. F. Edwards, *The Theory of Polymer Dynamics*, Oxford University Press, New York **1986**.
[42] D. Kawaguchi, K. Masuoka, A. Takano, K. Tanaka, T. Nagamura, N. Torikai, R. M. Dalgliesh, S. Langridge, Y. Matsushita, *Macromolecules* **2006**, *39*, 5180.
[43] A. Karim, A. Mansour, G. P. Felcher, T. P. Russell, *Phys. Rev. B* **1990**, *42*, 6846.
[44] S. J. Whitlow, R. P. Wool, *Macromolecules* **1991**, *24*, 5926.
[45] Y. Fujii, H. Atarashi, M. Hino, T. Nagamura, K. Tanaka, *ACS Appl. Mater. Interfaces* **2009**, *1*, 1856.
[46] T. Kumada, D. Miura, K. Akutsu-Suyama, K. Ohishi, T. Morikawa, Y. Kawamura, J.-i. Suzuki, T. Oku, N. Torikai, T. Niizeki, *J. Appl. Crystallogr.* **2022**, *55*, 1147.
[47] T. Kumada, D. Iwahara, S. Nishitsuji, K. Akutsu-Suyama, D. Miura, R. Motokawa, T. Sugita, N. Torikai, N. Amino, T. Oku, M. Takenaka, *J. Phys. Chem. C* **2024**, *128*, 8797.
[48] M. Hara, A. Kodama, S. Washiyama, Y. Fujii, S. Nagano, T. Seki, *Macromolecules* **2022**, *55*, 4313.
[49] J. L. Keddie, R. A. L. Jones, R. A. Cory, *Europhys. Lett.* **1994**, *27*, 59.
[50] J. A. Forrest, K. Dalnoki-Veress, J. R. Stevens, J. R. Dutcher, *Phys. Rev. Lett.* **1996**, *77*, 2002.
[51] E. K. Lin, R. Kolb, S. K. Satija, W.-l. Wu, *Macromolecules* **1999**, *32*, 3753.

[52] K. I. Akabori, K. Tanaka, A. Takahara, T. Kajiyama, T. Nagamura, *Eur. Phys. J.:Spec. Top.* **2007**, *141*, 173.
[53] K. Geng, R. Katsumata, X. Yu, H. Ha, A. R. Dulaney, C. J. Ellison, O. K. C. Tsui, *Macromolecules* **2017**, *50*, 609.
[54] J. Yan, J. Xu, L.-T. Weng, F. Wang, X. Wang, H. Yuan, T. Wang, O. K. C. Tsui, *Macromolecules* **2023**, *56*, 556.
[55] F. Brochard, J. Jouffroy, P. Levinson, *Macromolecules* **1983**, *16*, 1638.
[56] D. Kawaguchi, Y. Ohta, A. Takano, Y. Matsushita, *Macromolecules* **2012**, *45*, 6748.
[57] R. Stadler, L. de Lucca Freitas, *Colloid Polym. Sci.* **1986**, *264*, 773.
[58] L. G. Baxandall, *Macromolecules* **1982**, *1989*, 22.
[59] L. Leibler, M. Rubinstein, R. H. Colby, *Macromolecules* **1991**, *24*, 4701.
[60] N. L. Yamada, N. Torikai, K. Mitamura, H. Sagehashi, S. Sato, H. Seto, T. Sugita, S. Goko, M. Furusaka, T. Oda, M. Hino, T. Fujiwara, H. Takahashi, A. Takahara, *Eur. Phys. J. Plus* **2011**, *126*, 108.
[61] K. Mitamura, N. L. Yamada, H. Sagehashi, N. Torikai, H. Arita, M. Terada, M. Kobayashi, S. Sato, H. Seto, S. Goko, M. Furusaka, T. Oda, M. Hino, H. Jinnai, A. Takahara, *Polym. J.* **2013**, *45*, 100.
[62] A. Nelson, *J. Appl. Crystallogr.* **2006**, *39*, 273.
[63] S. Plimpton, *J. Comput. Phys.* **1995**, *117*, 1.
[64] A. T. Hagler, E. Huler, S. Lifson, *J. Am. Chem. Soc.* **1974**, *96*, 5319.
[65] P. Dauber-Osguthorpe, V. A. Roberts, D. J. Osguthorpe, J. Wolff, M. Genest, A. T. Hagler, *Proteins: Struct., Funct., Bioinf.* **1988**, *4*, 31.
[66] A. Einstein, *Ann. Phys.* **1905**, *17*, 549.